FWI imaging as an alternative view of the Brazilian pre-salt

Carlos Alberto da Costa Filho, Sergio Barragan, Benjamin Huard, Gregório Azevedo, Karine Pereira and Luis Cypriano, CGG

Abstract

Seismic imaging has traditionally been viewed as separate from, but dependent on, the inversion of velocity. Time-lag full-waveform inversion (TLFWI) has been shown to successfully invert for velocity even in the presence of cycle-skipping and amplitude mismatch in many geological environments. However, it has mostly been used to build a migration velocity model with low-to-mid frequencies, since migration kinematics are insensitive to high frequencies in the velocity model. Here, we explore performing TLFWI up to high frequencies, and derive an image directly from the inverted model, bypassing much of the preprocessing, as well as the migration step. We show two narrow-azimuth towed-streamer (NATS) examples from Santos Basin, one from a flat streamer acquisition, and another from a variable-depth streamer acquisition. They indicate that the nonlinear inversion of the full wavefield (i.e., including multiples and other phenomena) improves illumination and provides additional structural information when compared with conventional reverse-time migration (RTM), thus offering an alternative view of the Brazilian pre-salt.

Introduction

Brazilian offshore sedimentary basins such as the Santos Basin contain a significant fraction of the total hydrocarbon reserves in the world. These reserves may be situated above or below salt layers of varying degrees of complexity. As more easily accessible deposits in the post-salt are explored, the frontier shifts towards deeper targets located in the pre-salt layer.

Due to its performance in the presence of complex structures, full-waveform inversion (FWI) has become a popular tool in these areas for obtaining estimates of the subsurface velocity, mostly intended to be used in a migration. Further, time-lag FWI (Zhang et al., 2018) has proven to be an effective FWI algorithm to mitigate the complications caused by high geological complexity. When using these velocity models, reverse-time migration (RTM) is today the best and most widely used choice for imaging the Brazilian pre-salt. In the Santos Basin it has been used to vastly improve legacy velocity models using NATS (Barragan et al., 2019) and OBN data (Jouno et al., 2019).

Despite its successes, RTM is known to distort amplitudes in areas of high geological complexity and uneven illumination, especially when used with NATS data. One approach to correct these issues is to use least-squares RTM (LSRTM). LSRTM attempts to directly invert the linearized wave-equation Born modeling operation, for example, by using image-domain matching filters (Guitton, 2004; Wang et al., 2016).

Instead of using linear approximations, we exploit TLFWI to generate high-frequency velocity models, from which we extract impedances and create structural images of the subsurface (Zhang et al., 2020). These FWI images are possible for large models only due to the recent expansion in computational power. In contrast to migration, FWI imaging is a multi-scale, iterative, nonlinear inversion of the full wavefield, including surface and intrabed multiples, refractions and diving waves, in addition to primaries. TLFWI is also primarily driven by traveltimes, and thus, it is robust in the presence moderate cycle-skipping (Zhang et al., 2018; Wang et al., 2019). Moreover, it requires very little pre-processing. For example, time consuming steps such as demultiple and deghosting, are obviated.

Given the advantages of FWI imaging, we explore the potential of FWI imaging with narrow-azimuth (NAZ) acquisitions in two regions of moderate-to-high geological complexity in the Santos Basin, offshore Brazil. The first is a flat streamer NATS dataset, while the second is a variable-depth NATS dataset representative of more modern acquisitions, also from Santos Basin.

Time-lag FWI for imaging

The objective of a time-lag full-waveform inversion is to minimize the traveltime difference between synthetic and observed data (Luo and Schuster, 1991). It can be expressed as the minimization across all velocity models v of the following cost function (Zhang et al., 2018)

$$\chi(v) = \sum_{s,r,w} c\Delta\tau^2 \tag{1}$$

where s, r, w, c are respectively sources, receivers, time windows, and the correlation coefficient between synthetic and observed. The traveltime difference $\Delta\tau$ is defined as

$$\Delta\tau = \arg\max_{\tau} \int_{w} d^{\mathrm{obs}}(t+\tau)\, u[v](t)\, \mathrm{d}t \tag{2}$$

where $u[v]$ is the synthetic modelled from velocity v. The adjoint state method allows us to efficiently compute the gradient of (1), making it possible to minimize it using gradient-based methods (Plessix, 2006; Virieux and Operto, 2009).

Once the velocity model is obtained, one may estimate the reflector-normal reflectivity R using the following relation (Kalinicheva et al., 2020; Zhang et al., 2020):

$$R = \frac{\partial \ln \rho v}{\partial \vec{n}} \propto \frac{1}{v}\frac{\partial v}{\partial \vec{n}} \quad (3)$$

where $\vec{n}$ is the unit vector normal to the reflector and the density ρ is taken to respect Gardner's equation, $\rho = \alpha v^{\beta}$. Since our goal is to obtain a purely structural image, the exact choice of α and β is unimportant.

The quantity obtained in equation 3 is referred to as the FWI image (Zhang et al., 2020) and is equivalent to

$$R \propto \frac{1}{v}\nabla v \cdot (\sin\theta\cos\phi\,, \sin\theta\sin\phi\,, \cos\theta) \quad (4)$$

where θ and ϕ are dip and azimuth angles, obtained in practice via automatic scanning of local slopes.

Flat streamer NATS field data example

We perform FWI imaging using a legacy flat streamer NATS dataset from the Santos Basin. The acquisition contains offsets up to 6 km and usable frequencies above 4.5 Hz. Hence, this is a challenging dataset for FWI, which relies on low frequencies and long offsets to derive tomographic updates. These limitations are somewhat more relaxed for TLFWI, which has been shown to be robust with respect to moderate cycle-skipping and noise content. Nevertheless, it is important to perform velocity model building (VMB) using other techniques such as manual salt interpretation prior to TLFWI, to ensure the best possible starting model.

After the initial VMB, we perform TLFWI up to 18 Hz, as shown in Figure 1. It is possible to notice the high level of detail from the post-salt to the pre-salt, as expected from a fairly high-frequency TLFWI compared to conventional production inversions. This velocity model, or a lower frequency model kinematically equivalent to it, is what is commonly used to perform RTM.

In Figure 2a we show the RTM obtained by migrating processed data using our final FWI velocity model. Common in NAZ datasets, the RTM suffers from poor illumination in some regions, impacting interpretation of important features. Of particular interest, the base of salt (BOS) is poorly imaged in several locations where the salt exhibits high complexity, as shown by the yellow arrows. Salt flanks are also difficult to image, and this RTM is no exception, as shown by the white arrow. The pre-salt in this image is also affected, as can be observed by the discontinuous event indicated by the red arrow.

Alternatively, we may derive an FWI image directly from the FWI velocity model in Figure 1 by applying equation 4. It is immediately noticeable that regions indicated by the arrows are improved in this image. The strength and continuity of both the BOS and the pre-salt event, indicated by the red arrow, improved in the FWI image.. The salt flank, which previously contained almost no detail, could now be used for a more meaningful interpretation. Careful observation also reveals that some migration artifacts have been removed. In addition, both shallow and deep faults remain intact.

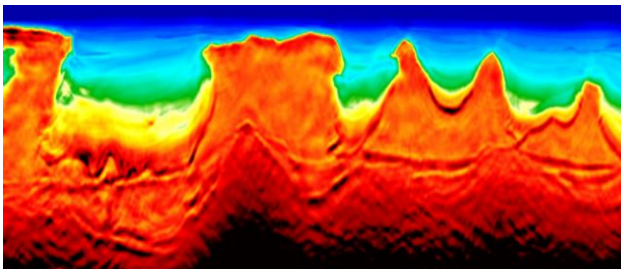

Figure 1. FWI velocity model for the flat streamer NATS.

It is important to remember that these images were obtained from very different procedures: RTM from a (linear) migration of processed data and the FWI image from an impedance calculation using a velocity model obtained by VMB which includes human interpretation. It is therefore natural to question whether the better imaged BOS in the FWI image is a consequence of our salt interpretation, rather than being obtained from the nonlinear inversion as we expect.

To quell this doubt, we show the FWI image obtained from the starting model containing human interpretation in Figure 3a and compare it to the FWI image obtained from the final, high-frequency velocity model in Figure 3b. The only VMB performed between these two velocity models was high-frequency TLFWI, thus the difference between these two images is entirely contributed by TLFWI. While the FWI image from the starting model contains some high-frequency content at the BOS, it is relatively weak compared to that of the final model. Indeed, high-amplitude, high-definition detail at the BOS and elsewhere is introduced by high-frequency TLFWI.

Variable-depth streamer NATS field data example

We also perform FWI imaging using a variable-depth streamer NATS dataset from the Santos Basin. This more modern acquisition contains offsets up to 8 km and usable frequencies as low as 3 Hz. These low frequencies were possible due to the variable-depth streamers, which staggers ghost notches and places receivers in a deeper, less noisy environment (Soubaras and Dowle, 2010).

Similarly to the previous example, we perform VMB including reflection tomography, manual interpretation and low-frequency FWI prior to high-frequency FWI. To obtain the FWI image, we ran TLFWI up to 16 Hz. Using the final velocity model, we obtain a 16 Hz RTM from the processed data as shown in Figure 4a. This image also features a broken BOS as indicated by the centermost arrow. The bottommost arrow indicated very weak pre-salt reflectors.

The FWI image is displayed in Figure 4b. It features more balanced top-down amplitudes and cleaner post-salt than RTM. In areas of interest such as the BOS, the FWI image is more continuous. In addition, the topmost arrow shows one region where migration artifacts appear in the RTM, but not in the FWI image. Moreover, the faults surrounding this noise have been preserved.

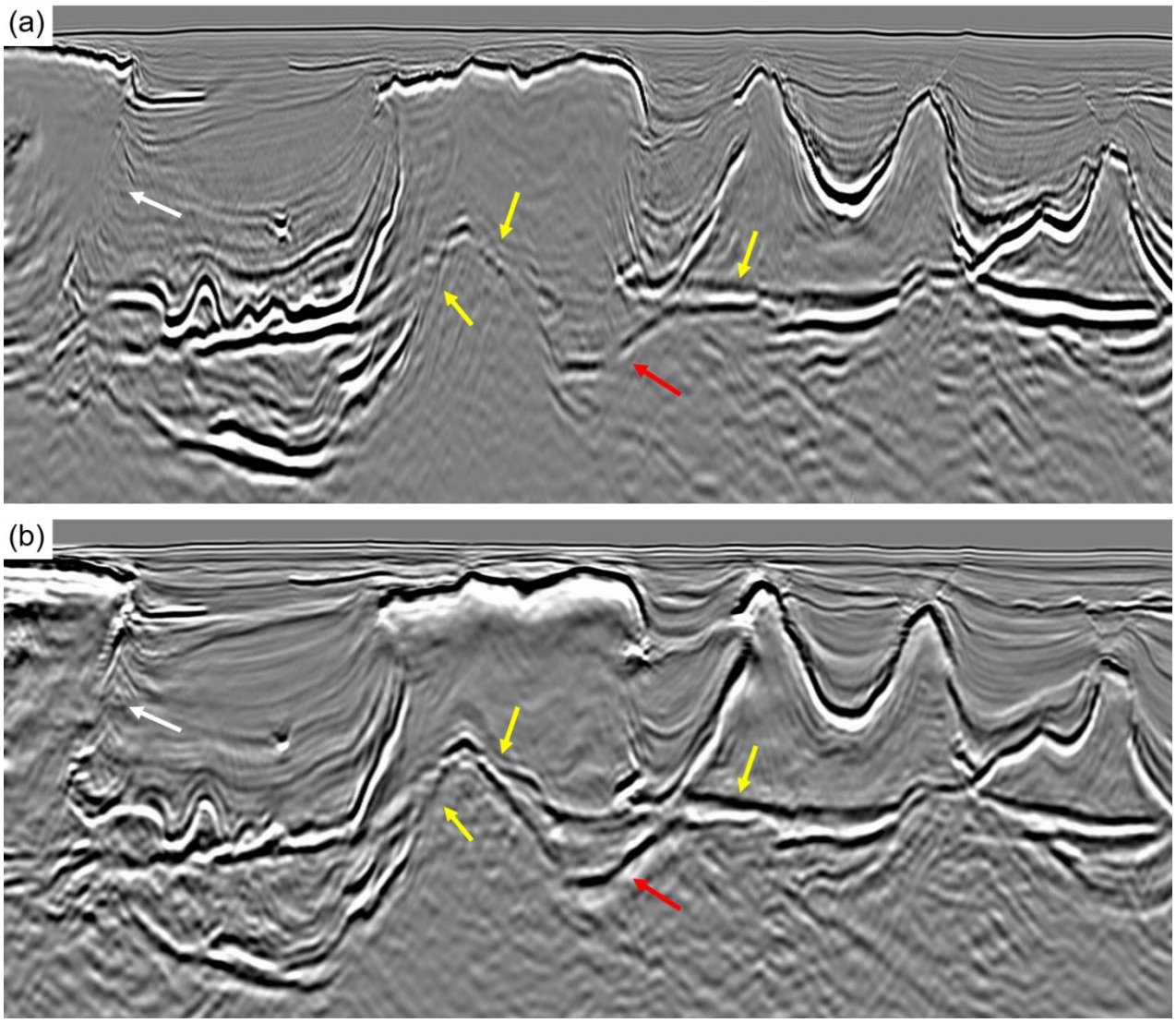

Figure 2. Inlines from the flat streamer NATS dataset (a) 18 Hz RTM image using velocity model in Figure 1. (b) 18 Hz FWI image derived from Figure 1 according to equation 4. Arrows indicate locations where the FWI image improves over RTM.

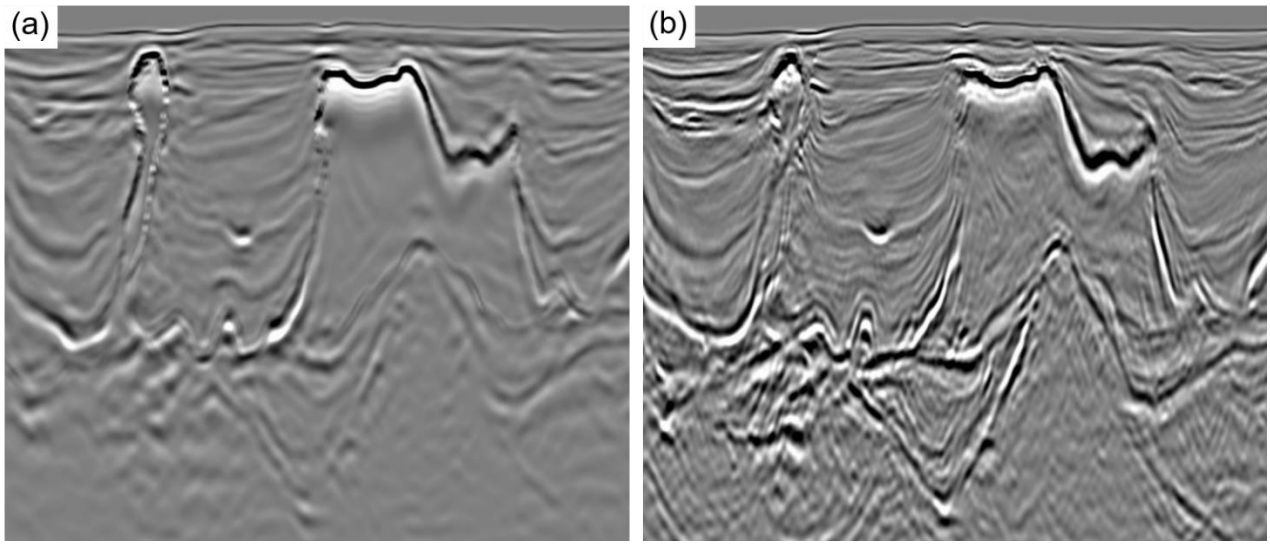

Figure 3. Inlines from the flat streamer NATS dataset. (a) FWI image of the initial model containing manual interpretation. (b) FWI image of the final, high-frequency model.

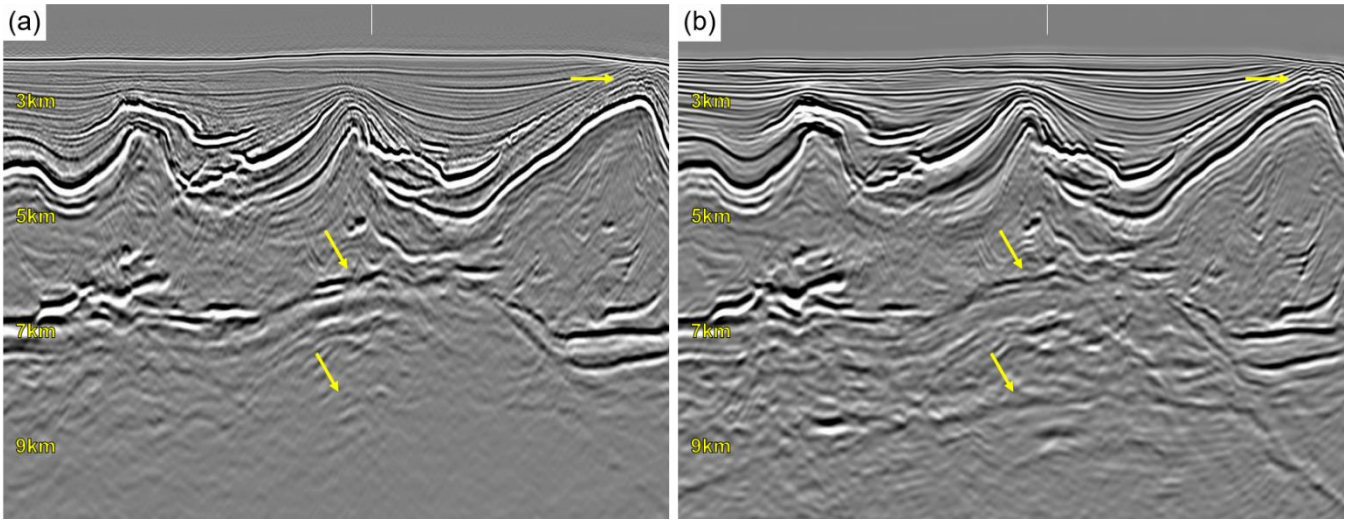

Figure 4. Inlines from the variable-depth NATS dataset: (a) 16 Hz RTM, and (b) 16 Hz FWI image. Vertical white lines on the top indicate position of crosslines in Figure 5. Features indicated by the arrows show improvements of FWI imaging over RTM, as discussed in text.

The structure indicated by the bottommost arrow is enlarged in Figure 5. It is very poorly imaged by RTM, appearing discontinuous and barely interpretable.

However, it appears in the FWI image as a coherent, continuous reflector visible across the entire inline.

The crossline view of this area as shown in Figures 6a and 6b adds further insights. The topmost arrows show an intra-salt region which is better imaged in the FWI image. The bottommost two arrows show two faults which appear distinctively in the FWI image but do not feature very prominently in the RTM.

A depth slice at 6.2 km of the RTM and FWI image and are shown respectively in Figures 6c and 6d. The locations of the inlines and crosslines discussed are indicated by the vertical and horizontal lines, respectively. At this depth, the structure surrounding their intersection is a structural high, well imaged by both methods. Some structures around it are not imaged well by RTM as shown by the arrows.

Despite the several improvements over the conventional RTM process, as shown in Figures 4–6, our FWI image also has some unwanted effects. In the pre-salt where diving waves do not reach and the signal-to-noise ratio is poorer, our FWI images are noisier. In addition, the BOS, despite being more continuous in many locations, is weaker in terms of amplitudes when compared to the RTM.

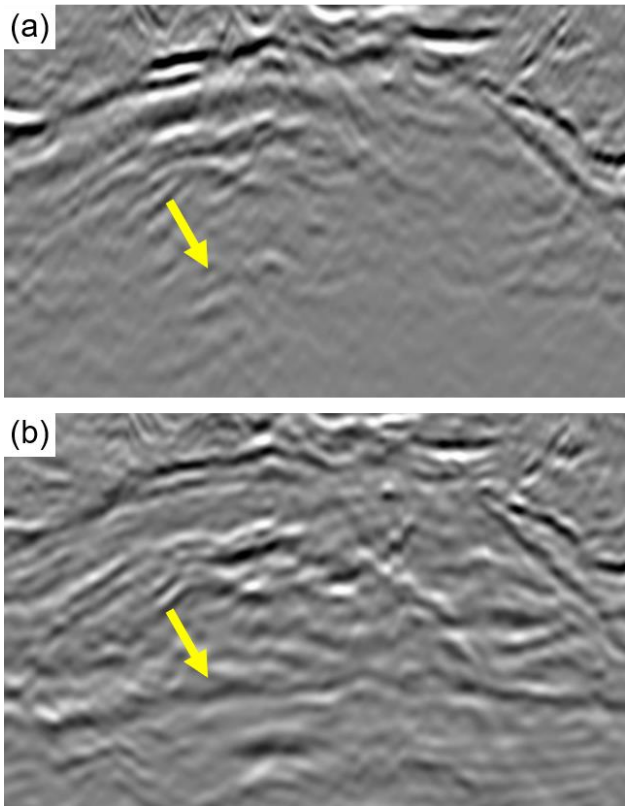

Figure 5. Magnified portion of Figure 4, comparing a pre-salt event in (a) RTM to (b) FWI image.

Discussion

With a maximum diving wave penetration of only a few kilometers (approximately 4 km in the second dataset), the inversions in the post-salt are high quality both in terms of kinematics and high-frequency events. In the salt and pre-salt, it is natural that TLFWI be more sensitive to the initial velocity model and inversion preconditioning.

Despite this, our results from both NATS datasets support the conclusion that TLFWI can better image some interesting pre-salt structures, if suitable velocities are provided for the salt and pre-salt. In this case, as direct consequence of the least-squares fitting and additional illumination provided by multiples and other nonlinear wave phenomena, FWI imaging can provide uplift in the form of more balanced amplitudes and better imaged events.

However, this uplift is also highly dependent on the data quality and may exhibit undesirable characteristics when used with data which has poor azimuthal coverage and poor low-frequency content. Non-linear events like

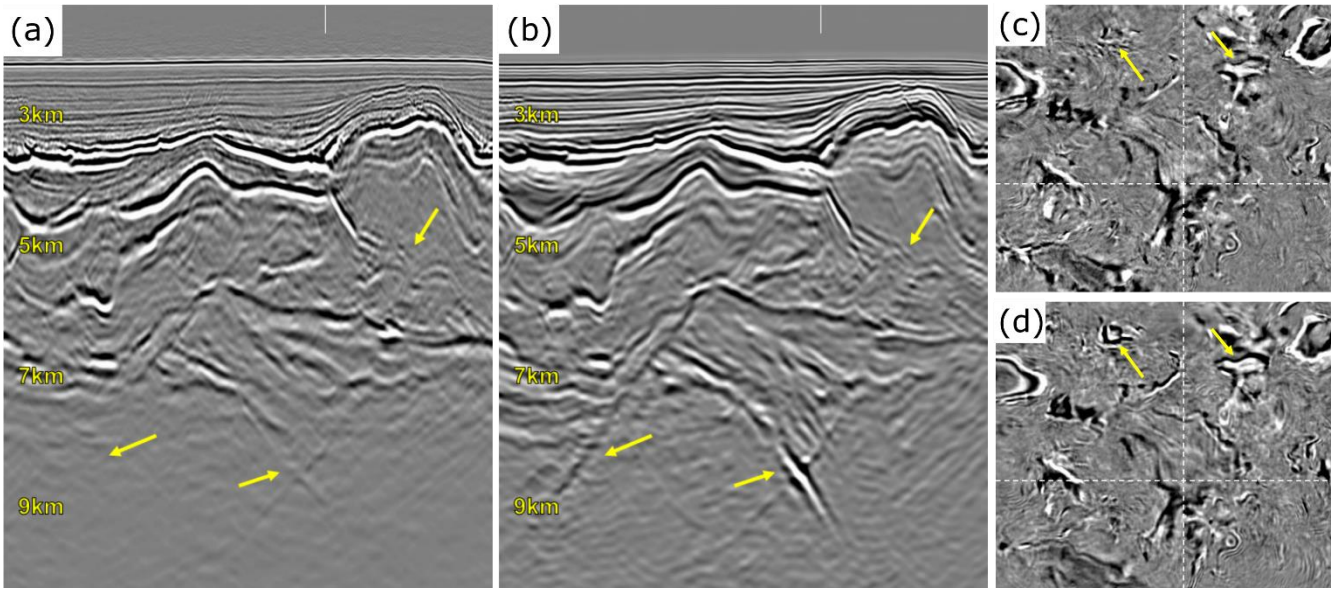

Figure 6. Crossline view of the variable-depth NATS dataset for (a) RTM and (b) FWI image. White dashed line indicates the location of the inlines of Figure 4. Depth slices at 6.2 km taken from (c) RTM and (d) FWI image. Vertical and horizontal white dashed lines indicate respectively the inline locations from Figure 4 and crossline locations of panels (a) and (b). Arrows indicate features discussed in the text.

multiples may have slow convergence rates and may create crosstalk in the FWI image. This greatly increases the dependence on the initial model. It helps direct the solution towards the correct global minimum rather than a local one. For similar reasons, the uplift also depends on the preconditioning/regularization used during inversion.

An additional limitation of the methodology is that simplified physics are used for modeling. No elastic or attenuative effects were modelled, and both our density and anisotropy models were not updated by FWI. Consequently, obtained reflectivities do not represent the subsurface exactly.

Conclusions

We have exploited time-lag full waveform inversion (TLFWI) to generate high-frequency velocity models whose short-scale variations are used to construct a structural image. Using two NATS datasets, one from flat streamer and another from variable-depth streamer, both from Santos Basin, we compared the FWI images to RTM. We observed that despite the limitations of NAZ datasets, we were able to image structures previously unseen in the pre-salt, which offered a completely novel view of this region.

Acknowledgments

The authors thank CGG for permission to publish this work and CGG MCNV for the Santos Basin datasets.

References

Barragan, S., D. Donno, F. Jouno, A. Martinez, and A. Khalil, 2019, Updating velocity models for complex pre-salt targets in Santos basin: Proceedings of the 16th International Congress of the Brazilian Geophysical Society & Expogef, 1–6.

Guitton, A., 2004, Amplitude and kinematic corrections of migrated images for nonunitary imaging operators: Geophysics, **69**, 1017–1024.

Jouno, F., A. Martinez, D. Ferreira, D. Donno, and A. Khalil, 2019, Illuminating Santos Basin's pre-salt with OBN data: Potential and challenges of FWI: SEG Technical Program Expanded Abstracts 2019, 1345–1349.

Kalinicheva, T., M. Warner, and F. Mancini, 2020, Full-bandwidth FWI: SEG Technical Program Expanded Abstracts 2020, 651–655.

Luo, Y., and G. T. Schuster, 1991, Wave-equation traveltime inversion: Geophysics, **56**, 645–653.

Plessix, R.-E., 2006, A review of the adjoint-state method for computing the gradient of a functional with geophysical applications: Geophysical Journal International, **167**, 495–503.

Soubaras, R., and R. Dowle, 2010, Variable-depth streamer – a broadband marine solution: First Break, **28**, 89–96.

Virieux, J., and S. Operto, 2009, An overview of full-waveform inversion in exploration geophysics: Geophysics, **74**, WCC1–WCC26.

Wang, P., A. Gomes, Z. Zhang, and M. Wang, 2016, Least-squares RTM: Reality and possibilities for subsalt imaging: SEG Technical Program Expanded Abstracts 2016, 4204–4209.

Wang, P., Z. Zhang, J. Mei, F. Lin, and R. Huang, 2019, Full-waveform inversion for salt: A coming of age: The Leading Edge, **38**, 204–213.

Zhang, Z., J. Mei, F. Lin, R. Huang, and P. Wang, 2018, Correcting for salt misinterpretation with full-waveform inversion: SEG Technical Program Expanded Abstracts 2018, 1143–1147.

Zhang, Z., Z. Wu, Z. Wei, J. Mei, R. Huang, and P. Wang, 2020, FWI Imaging: Full-wavefield imaging through full-waveform inversion: SEG Technical Program Expanded Abstracts 2020, 656–660.